

Phase Transition of Thin-Film Superconducting Cylinders in a Magnetic Field.

I. Parallel-Field Measurements*

L. Meyers†

Boston University, Boston, Massachusetts 02215

and

R. Meservey

Francis Bitter National Magnet Laboratory, Massachusetts Institute of Technology, Cambridge, Massachusetts 02139‡

(Received 3 February 1971)

The superconducting transition temperature was measured as a function of magnetic field for thin-film hollow cylinders in an accurately parallel magnetic field. Quantitative results were obtained for one indium and nine aluminum cylinders with film thicknesses d varying from 2900 to 340 Å and with diameters from 1.4 to 4.8 μ . The results agree well with Tinkham's analysis based on the Ginzburg-Landau theory even in the very-thin-film region where the penetration depth $\lambda \gg d$ and the transition region is greatly broadened. Values of λ obtained from the amplitude of periodic variations of T_c with H and from the background monotonic variation of T_c both agree with values derived from the low-temperature critical field and theoretical estimates. A search for higher-order electron correlations which would give an admixture of higher periodicity of flux quantization yielded a negative result. Evidence was found for the effect of fluctuations on the magnetic field dependence of the phase boundary.

I. INTRODUCTION

The discovery that in very small hollow superconducting cylinders the transition temperature is periodic with magnetic field was made by Little and Parks.^{1,2} Their measurements showed that the magnetic field period in cylinders of tin, aluminum, indium, lead, and tin-indium alloys corresponded approximately to the value expected from the quantization of magnetic flux in units of $hc/2e$. These results confirmed the somewhat prior discovery of flux quantization in superconductors by Doll and Näbauer³ and Deaver and Fairbank.⁴ Additional measurements have been made by Little,⁵ by Meyers and Little,⁶ by Groff and Parks,⁷ by Meservey and Meyers,⁸ and by Spence.⁹ The normal-superconducting phase boundary in the H, T plane was studied quantitatively by Groff and Parks⁷ for relatively thick aluminum films on small-diameter fibers; their results are in good agreement with theory.

The present investigation extends the range of quantitative data on aluminum to thinner films and larger diameters and gives some results on indium. We also describe observations of fine structure on the phase boundary, a search for higher-order correlations, and the probable observation of fluctuation effects. In the present experiment the magnetic field is aligned accurately parallel to the cylinder's axis. A subsequent paper will describe the angular dependence of flux quantization effects.

II. SUMMARY OF THEORY

The variation of the transition temperature of a small thin-film superconducting cylinder as a function of the magnetic field has been given by Tinkham¹⁰ on the basis of the Ginzburg-Landau theory. The result is similar to that used by Little and Parks¹ in analyzing their original experiment, but gives a numerically important correction and considers the case of a nonzero angle between the magnetic field and the axis of the cylinder.

The basic result of this theory is that the phase boundary between the normal and superconducting state of a thin-film cylinder is given by the following expression for H_c and $T_c(H)$:

$$T_c(H) = T_c(0) - \frac{T_c(0) R^2}{8\lambda_e^2(0) H_{cB}^2(0)} \left[\left(H \cos\theta - \frac{n\phi_0}{\pi R^2} \right)^2 + \frac{1}{3} \frac{d^2}{R^2} H^2 \cos^2\theta + 4 H^2 \sin^2\theta \right]. \quad (1)$$

In this expression $T_c(0)$ is the transition temperature for zero magnetic field, $T_c(H)$ is the transition temperature for an applied magnetic field H , and R is the mean radius of the cylinder, whose thickness d is assumed to be small compared with R . The angle θ is that measured between the direction of H and the axis of the cylinder.

In the part of the investigation reported here, only the case $\theta = 0$ will be considered. However,

even for $\theta = 0$, it is useful to have the full expression to determine the limit to which the alignment with field must be made in order that the expressions for $\theta = 0$ be valid. This is particularly true for small values of d/R , with which we are mainly concerned. To see how stringent the requirement for angular alignment can be, consider the case of $d = 500 \text{ \AA}$ and $R = 5 \mu$. Here the condition for the third term in the brackets in Eq. (1) being unimportant as compared with the second term is that the field be aligned within

$$\Delta\theta \ll d/2\sqrt{3}R = 2.9 \times 10^{-3} \text{ rad.}$$

Equation (1) is derived assuming the empirical temperature dependences

$$\lambda_e(t) = \lambda_e(0) (1 - t^4)^{-1/2} \quad (2)$$

and

$$H_{cB}(t) = H_{cB}(0) (1 - t^2), \quad (3)$$

where $\lambda_e(0)$ and $H_{cB}(0)$ are the penetration depth of the film and the bulk critical field both at $T = 0$.

In the present experiments the cylinder will always be exactly aligned with the magnetic field and so with $\theta = 0$, Eq. (1) becomes

$$\Delta t_c = \frac{T_c(0) - T_c(H)}{T_c(0)} = \frac{R^2}{8\lambda_e^2(0)H_{cB}^2(0)} \left[\left(H - \frac{n\phi_0}{\pi R^2} \right)^2 + \frac{1}{3} \frac{d^2}{R^2} H^2 \right]. \quad (4)$$

In this case, where $\theta = 0$, Douglass¹¹ has derived an expression containing additional higher-order terms, which, as slightly corrected by Groff and Parks⁷ and by Delmasso and Pagiola,¹² is

$$\Delta t_c = \frac{R^2}{8\lambda_e^2(0)H_{cB}^2(0)} \left\{ \left(H - \frac{n\phi_0}{\pi R^2} \right)^2 \left[1 + \left(\frac{d}{2R} \right)^2 \right] \right.$$

$$\left. + \frac{1}{3} \frac{d^2}{R^2} H^2 \left[1 + \frac{7}{5} \left(\frac{d}{2R} \right)^2 + O\left(\frac{d}{2R} \right)^4 \right] \right\}. \quad (5)$$

The equation is useful in determining the possible effects of certain higher-order terms, but actually the precision of present or previous experiments has not been sufficient to definitely detect these higher-order corrections. In practice, therefore, Eq. (4) is sufficient for most comparisons with measurements.

Equations (4) and (5) give n curves in the H, T plane corresponding to n different angular momentum states. Figure 1 shows these curves with the magnetic field H expressed in units of $\phi_0/\pi R^2$, where R is the mean radius of the cylinder and $\phi_0 = hc/2e$. It is assumed that the actual phase boundary corresponds to the value of the integer n which maximizes the critical temperature $T_c(H)$. Thus the normal state is to the right of the curve for the angular momentum state giving the highest value of $T_c(H)$ for a given applied magnetic field. The general features of the curve are particularly transparent in Eq. (4). Here, the first term in the parentheses gives a periodic cusplike oscillation of $T_c(H)$ and the second term gives a monotonic decrease in $T_c(H)$ proportional to H^2 . The latter term is the same as that caused by the screening effects if the cylinder had a break in it and was singly connected. The first term results from the constraint that the angular momentum must be quantized in a doubly connected superconductor.

Some properties of Eq. (5) which will be useful in the analysis of the experiments will be noted.⁷ By setting $d(\Delta t_c)/dH = 0$ we find the local maxima in $T_c(H)$ to be at

$$H_{\max} = \frac{n\phi_0}{\pi R^2} \left[1 - \frac{1}{3} \frac{d^2}{R^2} + O\left(\frac{d^4}{R^4} \right) \right], \quad (6)$$

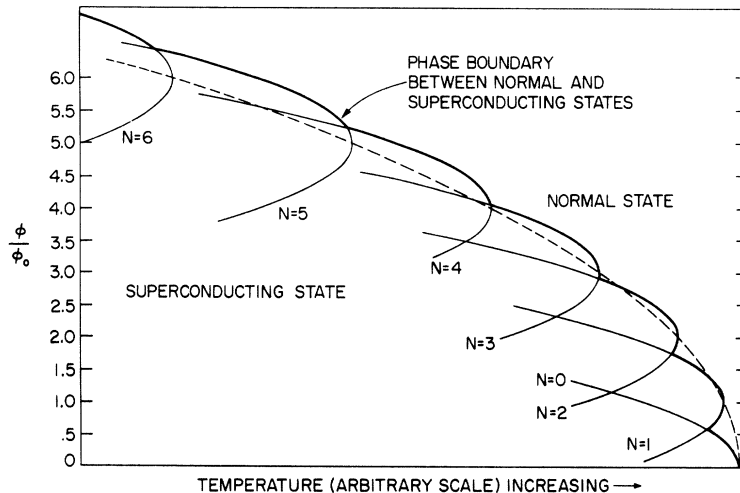


FIG. 1. Theoretical phase boundary for a hollow thin-film superconductor as a function of temperature and enclosed magnetic flux (units of $\phi_0 = hc/2e$). The numbers denote angular momentum states; the state with the highest value of T for a given value of ϕ determines the transition temperature. The dotted background parabola connects the maximum values of T for each angular momentum state.

and the difference between local maxima in $T_c(H)$ is, according to Eq. (5), completely independent of H . Neglecting terms of the order d^4/R^4 , a parabola which passes through these local maxima is given by

$$(\Delta T_c)_B = \left(\frac{d^2}{24\lambda_e^2(0)H_{cB}^2(0)} \right) H^2. \quad (7)$$

This background curve, which it should be noted is not the envelope of the individual curves for each quantum number, is just what we would observe for a singly connected film. For $n=0$ we also have a parabola (except for high-order terms) given by

$$(\Delta t_c)_{n=0} = \left(\frac{R^2}{8\lambda_e^2(0)H_{cB}^2(0)} \right) H^2 \left[1 + \frac{7d^2}{12R^2} + O\left(\frac{d^4}{R^4}\right) \right]. \quad (8)$$

The ratio of the quadratic coefficients of these two parabolas, that of the periodic term and that of the background term, is

$$\frac{(\Delta t_c)_{n=0}}{(\Delta t_c)_B} = \frac{3R^2}{d^2}, \quad (9)$$

again neglecting terms of order d^4/R^4 .

The values of H for which we have a local minimum in T_c are

$$H_{\min} = (n + \frac{1}{2}) \phi_0 / \pi R^2. \quad (10)$$

For $n=0$ the value of Δt_c at this minimum in T_c where the $n=0$ and $n=1$ curves intersect is

$$(\Delta T_c)_m = \left(\frac{R^2}{8\lambda_e^2(0)H_{cB}^2(0)} \right) \times \left\{ \left(\frac{\phi_0}{\pi R^2} \right)^2 \left[1 + \frac{d^2}{3R^2} + O\left(\frac{d^4}{R^4}\right) \right] \right\}. \quad (11)$$

From Eqs. (6) and (10) we see the local maximum for n equals the local minimum for $n-1$ at

$$n = 3R^2/2d^2. \quad (12)$$

For H larger than that corresponding to this quantum number, there will be no local maximum in Δt_c , but this does not imply that the modulation of the background curve caused by flux quantization will end at this point.

The penetration depth λ used to obtain Eq. (1) or (4) was assumed to have the empirical temperature dependence given in Eq. (2) with $\lambda_e(0)$ a known constant. Actually the correct temperature dependence and absolute value that should be used is not a very simple question especially for thin films and deserves some discussion.

Consider first the temperature dependence of the penetration depth. The temperature dependence from Eq. (2) in the limit $T \rightarrow T_c$ is

$$\lambda_e(T) = \lambda_e(0)/2[(T_c - T)/T_c]^{1/2}. \quad (13)$$

This is the form used to obtain Eqs. (1) and (4) and $\lambda_e(0)$ is the empirical penetration depth at $T=0$ which must be found from other measurements. On the other hand, the microscopic BCS theory for a pure bulk superconductor gives for λ in the limit $T \rightarrow T_c$

$$\lambda(T) = \lambda_L(0)/\sqrt{2}[(T_c - T)/T_c]^{1/2}. \quad (14)$$

Here $\lambda_L(0)$ is the London penetration depth as defined by the BCS theory.¹³ Actually, however, the superconductors of interest have nonlocal electrodynamics in the bulk and the above equation does not apply. Miller¹⁴ has given the following equation for the penetration depth of a nonlocal superconductor when the mean free path $l \ll \xi_0$ and $T \rightarrow T_c$:

$$\lambda(T) = \lambda_L(0) [(2\hbar V_F k T_c) / (\pi \Delta^2(T) l)]^{1/2}. \quad (15)$$

This can alternately be written as

$$\lambda(t) = (0.605)\lambda_L(0) (\xi_0/l)^{1/2} (1-t)^{-1/2}. \quad (16)$$

This is the same as Eq. (13) with

$$\lambda_e(0) = (\xi_0/l)^{1/2} \lambda_L(0) \quad (17)$$

and a 20% change in the constant. According to de Gennes and Tinkham¹⁵ in the case of a thin film where $d < l \ll \xi_0$, which should apply in at least the thinner of the present films,

$$\lambda_e(0) = (\xi_0/d)^{1/2} \lambda_L(0). \quad (18)$$

The left-hand side of Eq. (4), which gives the depression in the transition temperature, is the result of taking the limit as $t \rightarrow 1$ of $\lambda_e^2(t)H_{cB}^2(t)/\lambda_e^2(0)H_{cB}^2(0)$ using the empirical temperature dependences given in Eqs. (2) and (3). For the BCS theory the limiting values as $t \rightarrow 1$ for $H_{cB}(t)$ and $\lambda_e(t)$ differ somewhat from the empirical expressions. Both temperature dependences are summarized in Table I.

Since Eq. (4) is the condition for the change in transition temperature because of the magnetic field, the last column in Table I is to be identified with the left-hand side of Eq. (4) with $(1-t) = \Delta t_c$. The net result is to show that using the proper microscopic expressions in place of the empirical ones makes only a small change in Eq. (4). The functional dependence of Δt_c on H remains the same, but its magnitude is decreased slightly. Thus Eq.

TABLE I. Temperature-dependent quantities as $T \rightarrow T_c$.

	$[H_{cB}(t)]_{t \rightarrow 1}$	$[\lambda_e(t)]_{t \rightarrow 1}$	$\left[\frac{H_{cB}^2(t)\lambda_e^2(t)}{H_{cB}^2(0)\lambda_e^2(0)} \right]_{t \rightarrow 1}$
Empirical	$2H_{cB}(0)(1-t)$	$\frac{1}{2}\lambda_e(0)(1-t)^{1/2}$	$(1-t)$
BCS	$1.74H_{cB}(0) \times (1-t)$	$0.605\lambda_e(0) \times (1-t)^{-1/2}$	$1.12(1-t)$

(4) should be corrected by replacing the 8 in the denominator of the right-hand side by 8.95.

In practice, since $\lambda_L(0)$ is not a measured quantity, the penetration depth can be obtained from the measured critical field of the thin film by using the Ginzburg-Landau expression for the critical field of a very thin film:

$$H_c(T) = (\sqrt{24}) H_{cB}(T) \lambda_e(T)/d. \quad (19)$$

de Gennes and Tinkham,¹⁵ using the microscopic theory, modify this result only slightly and give for $T=0$

$$H_c(0) = 5.8 H_{cB}(0) \lambda_e(0)/d. \quad (20)$$

They also find that for thin films the two-fluid temperature dependence,

$$H_c(t) = H_c(0) [(1 - t^2)/(1 + t^2)]^{1/2}, \quad (21)$$

is very close to the microscopic temperature dependence over the entire range of temperature. These equations allow us to deduce $\lambda_e(0)$ from measurements of $H_c(T)$ and d .

Although the value of $H_{cB}(0)$ is known for bulk superconductors, the quantity which we really need in Eq. (4) is the binding energy of the superconducting pairs per unit volume of the film. For aluminum films T_c increases approximately as $1/d$ and the energy gap increases correspondingly. As a first-order correction to $H_{cB}(0)$ to allow for the increase in binding energy it is reasonable to use an empirical relation which approximately relates $H_{cB}(0)$ of different superconductors to their transition temperatures T_c :

$$H_{cB_1}(0)/H_{cB_2}(0) = (T_{c1}/T_{c2})^{1.26}. \quad (22)$$

This empirical equation is obeyed rather well by common superconductors and was used to obtain the corrected value of the bulk critical field, $H_{cB}(0)$, used in Eq. (4) when comparing with thin-film measurements.

III. EXPERIMENTAL PROCEDURE

A. Preparation of Samples

The samples were prepared by evaporating high-purity (99.999% pure) aluminum or indium from a tungsten filament onto rotating quartz fibers located about 25 cm directly above the filament. The 12-in.-diam glass bell jar was evacuated with a 2400-liter/sec 6-in. diffusion pump, with a large "creep-free" liquid-nitrogen cold trap between the pump and the evaporation chamber. Before starting the evaporation the pressure in the evaporation chamber was reduced to 5×10^{-7} torr. During evaporation the pressure rose to about 2×10^{-5} torr for aluminum and about 10^{-6} torr for indium. The evaporation rate for both aluminum and indium was such that at the fiber position about 300 Å/sec would be

deposited on a nonrotating flat surface perpendicular to the flux of the evaporant.

The quartz fibers were prepared by a method very similar to that described by Strong.¹⁶ Starting with a 6-in. length of quartz rod, about 1 mm in diameter, the center section is heated to the softening point in an oxyacetylene flame. Immediately the two ends are pulled apart, producing two needlelike sections. Next, one "needle" is placed in the flame, parallel to the long dimension of the flame. The needle immediately melts and the jet action of the flame carries the molten quartz outward producing a long fine fiber that is recoverable in strong illumination. Many fibers were prepared with diameters in the range 0.6–6.0 μ and from among these a fiber of suitable diameter was chosen by observation in an optical microscope with a filar eyepiece. Because of diffraction effects this measurement was not very accurate. The fiber radius R reported in this paper was in each case calculated from the measured magnetic field periodicity ΔH and the theoretical flux quantum $\phi_0 = hc/2e = 2.07 \times 10^{-7}$ G cm², assuming the relation $\Delta H \pi R^2 = \phi_0$.

The special substrate used to support the fiber is shown in Fig. 2. These substrates were cut from a 1-mm-thick fused-quartz slide, using a glass saw. The fiber was stretched across a slot about 0.5 mm wide, and the substrate was bevelled below the fiber, so that during evaporation the flux of metal atoms was very nearly uniform on every part of the fiber (i. e., there was no significant shadowing). Before mounting the fiber on the substrate, two dots of silver paint (du Pont high-temperature silver paint No. 4666¹⁷) shown at A on Fig. 2 were baked onto the substrate at a temperature of 500 °C. After the metal evaporation, thin copper wires were soldered to A using Alpha No. 903 alloy solder.¹⁸

The unmetallized quartz fiber was mounted on the substrate by stretching it across the slot as shown in Fig. 2 and applying two dots of air-drying silver paint (du Pont No. 4817¹⁷) at B. This paint dried rapidly enough so that after 15 min the fiber

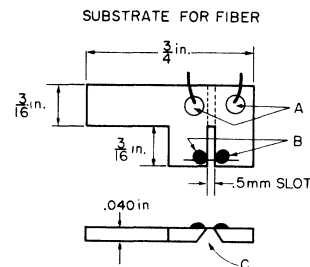


FIG. 2. Fused quartz substrate used to support fiber during metallization and measurement. A and B are silver paint spots used to attach the leads and the fiber, respectively.

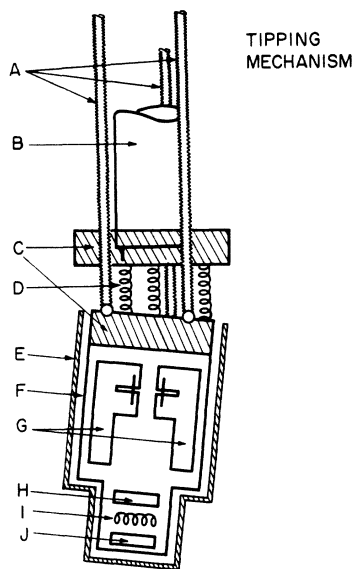


FIG. 3. Schematic view of the lower section of the Dewar insert with two substrates *G* in position on a plastic holder *F*, whose base plates *C* working against springs *D* can be tipped in two perpendicular directions by control screws *A*. On the sample holder are two resistance thermometers *H* and *J* and a noninductively wound heater *I*. *E* is a copper can which provides electrostatic shielding for the samples and the stainless-steel support tube *B* shields the leads to the samples.

remained taut without other aid. Before metallizing the fiber, a 0.05-mm-thick band of gold sheet was wrapped completely around the dashed area shown in the figure. The purpose of the band was to prevent evaporated metal from short circuiting the two ends of the fiber; the band was removed after evaporation.

B. Measurement Technique

The special substrates carrying the completed fibers were mounted on the substrate holder shown in Fig. 3. This holder was constructed so that the axis of the fiber could be tipped through several degrees about two perpendicular axes by rotating two stainless-steel control rods which passed through vacuum seals at the top of the cryostat. The angle of the fiber could be changed reproducibly by an angle as small as 3×10^{-4} rad. Two carbon resistance thermometers of nominal 10- and 50- Ω values and a 200- Ω noninductively wound nichrome wire heater were mounted on the holder to measure and control the temperature. The substrate holder was contained in a copper can to provide electrostatic shielding. Twisted copper leads from the samples passed through stainless-steel tubes to the top of the cryostat to provide separately shielded voltage and current leads to the samples and ad-

ditional shielded leads for the heater and thermometers.

The substrate holder was held in position near the bottom of a glass helium Dewar with the samples immersed in the liquid helium. On the outside of the helium Dewar was fitted (see Fig. 4) a copper solenoid which provided the magnetic field; the solenoid was immersed in the liquid nitrogen.

The helium bath was normally pumped on by a mechanical pump which gave temperatures down to 1.12 K. A 6-in. booster diffusion pump was available for temperatures down to 0.87 K when necessary. In the bottom of the helium Dewar was located another resistance wire heater to give convective circulation when measurements were made above 2.17 K, the superfluid transition temperature of helium. The Dewar assembly was surrounded by a $\frac{1}{16}$ -in.-thick 6-in.-diam shield of Moly-Permalloy¹⁹ to provide magnetic shielding.

The solenoid, which provided up to 430 G at the sample, was a sixth-order copper solenoid. The magnetic field over the region in which the samples were located (± 1 mm from the center in the axial direction and within 2.5 mm of the axis in the radial direction) had a theoretical variation of 1 part in 10^9 and in practice was negligible. The magnet current was supplied by a motor driven bipolar power supply to provide symmetrical sweeps of the magnetic field *H* through zero. The current through a 1- Ω resistor in the magnet circuit pro-

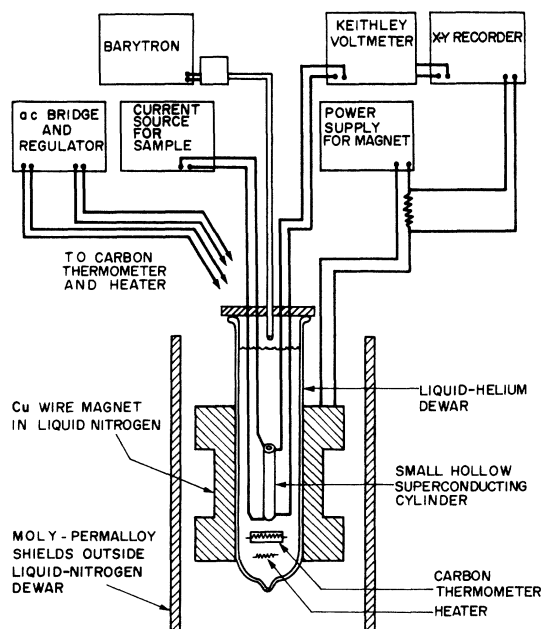


FIG. 4. Schematic diagram of the experimental arrangement.

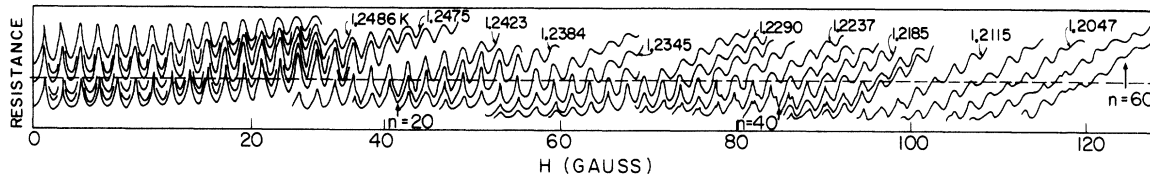


FIG. 5. Recorder traces of resistance versus magnetic field for closely spaced temperatures from which Fig. 6 was constructed. The dashed line represents the value of resistance ($0.45R_N$) chosen to represent the phase boundary.

vided the recorder with a voltage proportional to H . The solenoid was calibrated with a rotating coil gaussmeter and its uniformity tested with a Hall-effect probe.

The temperature of the liquid helium was measured by a 33-Hz resistance bridge.²⁰ A 10- Ω carbon resistor was used for temperatures below 1.5 K and a 50- Ω carbon resistor was used at higher temperatures. These resistance thermometers were calibrated on each run against an oil manometer in the He-II region and a Wallace and Tierman²¹ dial pressure gauge at higher temperatures. A pressure measuring instrument using a bellows and a capacitance sensor (MKS Barytron Gauge²²) was used to give a voltage proportional to the pressure recorder plots against this variable, which could be readily converted to temperature.

The current source for the sample was a mercury battery with a series resistance which gave currents up to 10 μ A, which were measured by a dc microammeter. The voltage was measured with a battery operated dc voltmeter (Keithley 147).²³ Voltage and current leads were individually shielded and the measuring circuit was completely isolated from the ac line except for the recorder whose power was obtained from an isolation transformer.

After mounting the samples, their resistance was measured at room temperature, at liquid-nitrogen temperature (≈ 77 K), and, after filling with liquid helium, at 4.2 K. As the temperature of the liquid helium was lowered below 4.2 K the resistance as a function of pressure was plotted on the x - y recorder using the Barytron gauge to provide a voltage proportional to pressure. The pressure was lowered until the sample passed through its superconducting transition and showed no more resistance. A measuring current of 1.0 μ A was standardly used and it was checked to see if increasing or decreasing this current by a factor of 3 changed the shape of the curve.

After the position of the transition was located, the temperature was adjusted to be in the steepest part of the transition, where the value of the resistance was about one-half the normal resistance, $R_N/2$. The temperature regulator was locked on to maintain this temperature constant to within about $\pm 10^{-5}$ K. The magnetic field was then increased and

the resistance would pass through a number of oscillations superimposed on a monotonically rising background. The angular position of the sample was then changed in such a way as to decrease the resistance by reducing the component of magnetic field perpendicular to the axis of the cylinder. By successively increasing the magnetic field and adjusting the angular position of the sample about the two orthogonal horizontal axes to a minimum resistance, the sample could be aligned in a relatively high field with great accuracy. After this initial alignment the temperature was raised briefly above T_c to eliminate any flux trapped in the cylinder and a final alignment made in the same way but starting with the cylinder almost exactly aligned.

Once the cylinder was aligned with the magnetic field the phase boundary was mapped out by one of two procedures. For smaller diameter samples where the changes in transition temperature were comparatively large so that there was good long-term stability in the measured resistance at a given

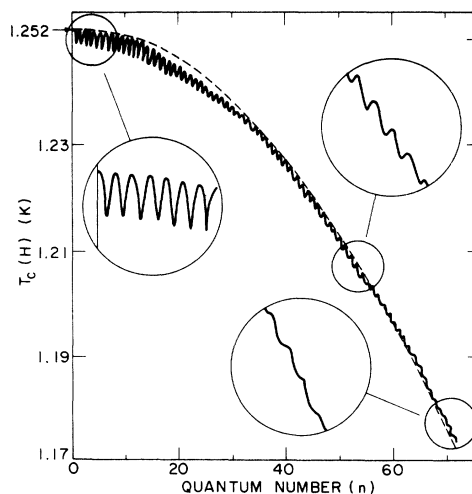


FIG. 6. Measured phase boundary for a thin-film aluminum cylinder 1030 \AA thick, 1.78- μ radius. T_c as a function of the magnetic field as measured in units of quantized flux (magnetic field change per quantum = 2.07 G). Insets show enlarged view of the phase boundary in three regions. Dashed line is a parabola fitted to the measured curve at $n=0$ and $n=50$.

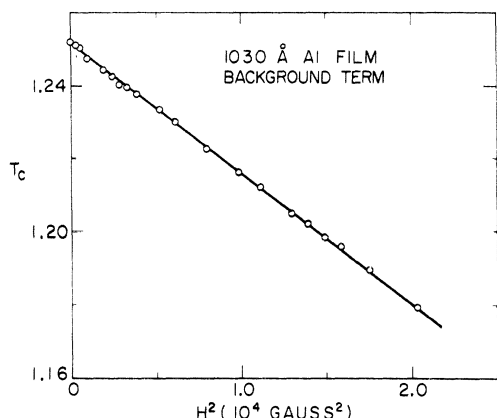


FIG. 7. Temperature plotted against the square of the magnetic field for the local temperature maxima for the sample of Figs. 5 and 6.

value of H and T , the resistance R as a function of H for closely spaced values of constant T was plotted on the x - y recorder. An example of such a family of curves is shown in Fig. 5. If we chose a given value of the resistance to define the phase boundary, for instance, $R = R_N/2$, the intersection of the line $R = R_N/2$ gives various values of H and T on the boundary. If the successive temperature traces are closely spaced, additional interpolated values of H and T on the phase boundary can be found until a complete curve of the locus of H and T for a given value of R can be constructed. The effect of changing the arbitrarily chosen value of resistance was also investigated. The limitations and complications of determining the phase boundary in this way will be discussed later.

For larger-diameter cylinders where the voltages involved were smaller and the long-term stability of temperature and magnetic field would not allow

many successive recorder traces, the phase boundary was plotted out point by point. Starting at $T = T_c(0)$, the transition temperature for $H = 0$ (defined, for instance, as the point at which $R = R_N/2$), the temperature would be successively lowered and the field changed to obtain the same resistance.

Using the temperature regulator and the resistance bridge small changes in temperature could be rapidly and conveniently made. The magnetic field would then be changed until the original resistance was recovered. At intervals the point at $T = T_c(0)$, $H = 0$ was checked to eliminate the effect of drift.

For some of the films the critical magnetic field was measured at a series of temperatures down to the lowest temperatures available ($T = 0.87$ K) using a magnet giving up to several kG. These data were used to calculate the penetration depth of the film.

The dimensions of the film were measured optically. The length (≈ 1 mm) could be determined by a measuring microscope. The diameter was determined approximately by a micrometer filar eyepiece on an optical microscope, but because of diffraction effects, this measurement was not accurate enough to use in analyzing the results. The diameter used was that calculated theoretically assuming the correctness of flux quantization in units of $hc/2e$. The thickness of the evaporated film was measured by the method of equal chromatic order. A step was made by scribing away a portion of the film on the flat fused quartz substrate and overcoating with silver. Provided the sticking coefficients of the quartz fiber and the quartz substrate are the same, the thickness of the evaporated cylinder on the fiber should equal that of the plane film on the substrate. This was the assumption made.

IV. RESULTS

A. Phase-Boundary Measurements

Figure 6 shows the measured phase boundary for

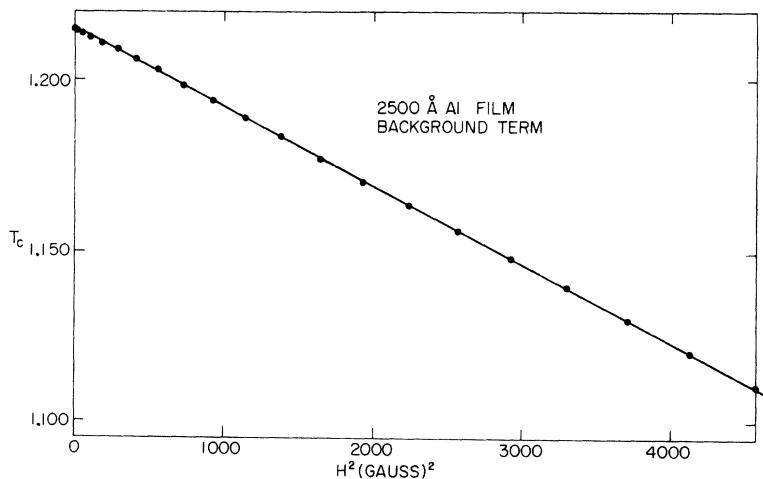


FIG. 8. $(T_c)_{\max}$ versus H^2 , 2500-Å aluminum film.

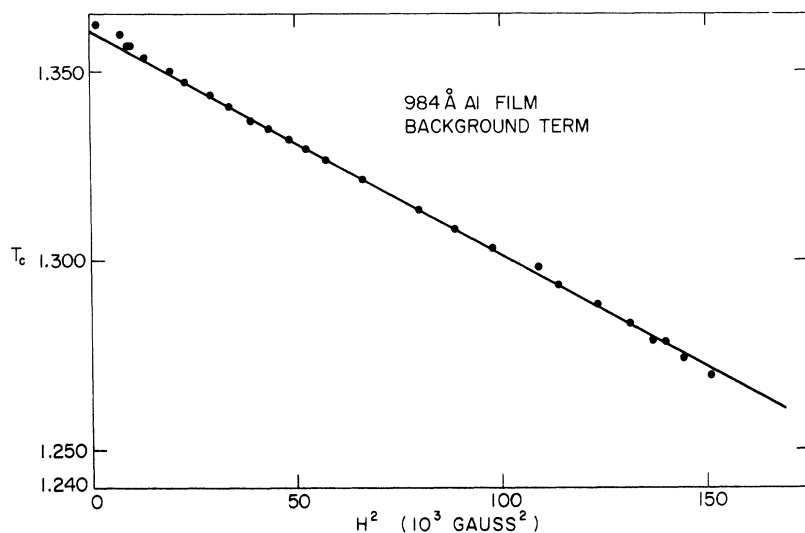


FIG. 9. $(T_c)_{\max}$ versus H^2 , 985-Å aluminum film.

an aluminum film 1030 Å thick with a radius of 1.78μ . The general form of the boundary is evidently as predicted by theory. To a first approximation, sections of parabolas are arranged on a parabolic background essentially as shown in Fig. 1. The shape of the curve is similar to that found by Groff and Parks,⁷ although the phase boundary has been measured to much higher quantum numbers. In fact the measurements extend beyond the point at which the measured local maxima in T_c disappear because of the steep background, and the different angular momentum states are only marked by discontinuities in slope. For this particular sample the highest angular momentum state that could be detected was $n = 75$ and to observe these high-numbered states it was important to have the sample exactly aligned with the magnetic field. The

shape of the variations of T_c for different regions of quantum number is shown by the enlarged insets. A closer inspection of Fig. 6 shows that there are deviations from the predicted parabola defined by the maxima in $T_c(H)$. In addition the amplitude of the oscillations falls off more rapidly with n than is predicted by Eq. (4).

Figure 5 shows for this same film some of the original data from which the phase boundary was constructed. The resistance as a function of magnetic field was recorded at a series of temperatures. The background curve (connecting the maxima in T_c) was constructed from the values of T and H at the resistance minima lying on the $R = 0.45 R_N$ line (dashed line in Fig. 5). Additional points could be obtained by interpolating the temperature between two resistance minima on each side of this

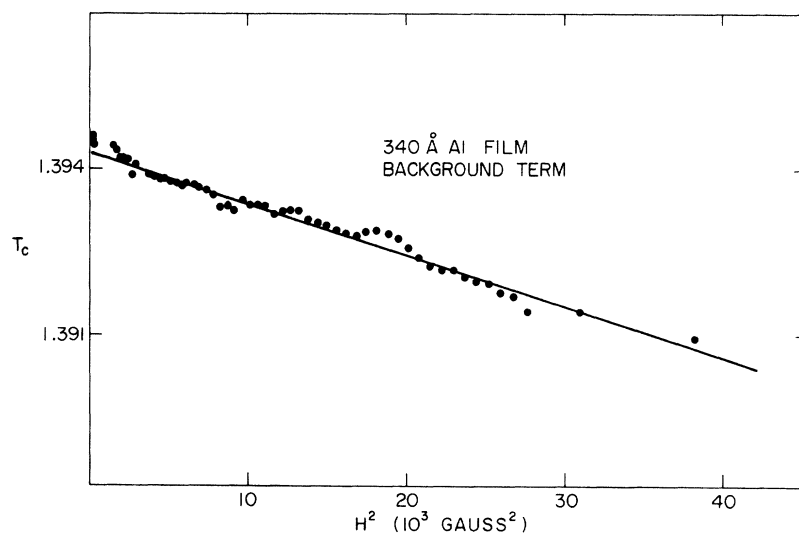


FIG. 10. $(T_c)_{\max}$ versus H^2 , 340-Å aluminum film.

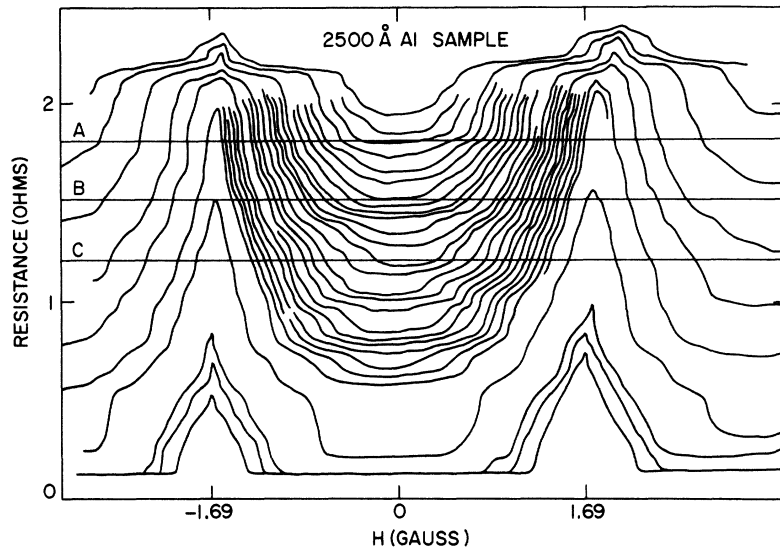


FIG. 11. Resistance vs magnetic field near $H=0$ for closely spaced temperatures. A, B, C are three different resistance levels used to construct the phase boundary.

value of resistance and close enough to it to be in a region where the resistance was linear in temperature at a given field. In Fig. 5 curves at intermediate temperatures are not shown for the sake of clarity. The minima in T_c can be plotted out in a similar manner. Given these reference points for each angular momentum state and the fact that there is a resistance region over which resistance is a linear function of temperature, the entire phase boundary can be made up of interpolated segments of such tracings. Figure 6 was constructed in this way.

Figure 7 shows the maxima of T_c plotted against the square of the corresponding magnetic field. The result is a straight line in agreement with the prediction of Eq. (4). Similar results are shown for other films of different thickness in Figs. 8-10 for a sample thickness of 2500, 984, and 340 Å, re-

spectively. In all samples measured, the transition temperature was depressed an amount proportional to H^2 over the entire range of fields where maxima could be distinguished. The considerable scatter in the case of the 340-Å film was associated with a rather broad transition with considerable structure.

The same technique for mapping out the phase boundary was applied in detail to the zero-angular-momentum state in many of the samples. Figure 11 shows the resistance curves as a function of magnetic field made for many closely spaced values of the temperature. Close to the normal resistance, which is approximately at the level of the maximum of the highest curve, the peculiarities of the curves are associated with structure on the highest position of the transition curve. This region will be discussed later but will be ignored at present. The lowest resistance of the curves corresponds to the

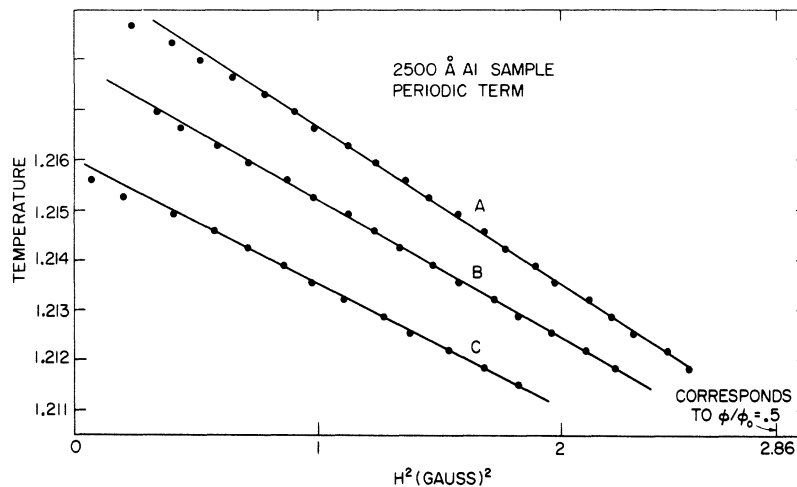


FIG. 12. T_c versus H^2 from the data of Fig. 11 show the periodic term ($n=0$) for the three choices of resistance.

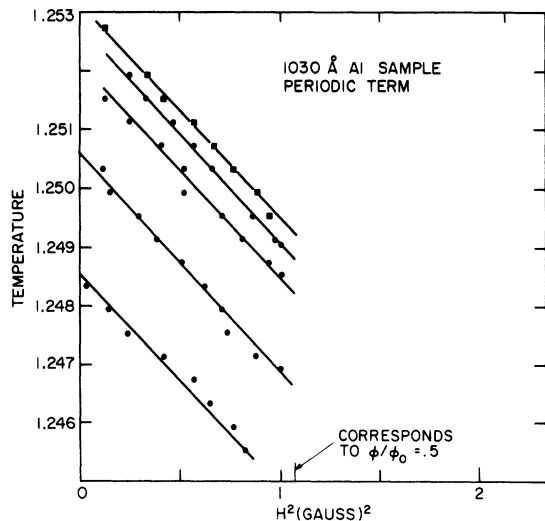


FIG. 13. T_c versus H^2 , 1030-Å aluminum film.

superconducting state. In this instance a slight resistance of the leads accounts for the finite measured resistance at low temperatures. The horizontal lines are three different resistance levels, the lowest chosen to be approximately in the center of the steep part of the transition curve near $R = R_N/2$ and the other two at higher resistance levels. By plotting the temperature and magnetic field at the intersection of these lines with those of constant temperature we obtain three plots of the "phase boundary" as shown in Fig. 12. Here the points determining line C came from the intersections of the lowest resistance curve of Fig. 11. The points determining lines B and A came from the intersections of the two higher resistance curves. It

is evident because of the finite width of the transition that there is no unique phase boundary defined by the resistance. (It should be mentioned that the resistance transition width of this particular film was what is usually considered rather sharp for evaporated films being about 0.009 K.) In spite of the fact that the position of the phase boundary is not unique, Fig. 12 shows that the depression of T_c is proportional to H^2 as expected from Eq. (4) with $n=0$. There is a slight progression of the slope between curves C, B, and A, whose cause is not known.

A similar plot of the periodic term ($n=0$) is shown in Fig. 13 for the 1030-Å-thick sample. Here the somewhat more scattered results give an average quadratic behavior with the slope almost constant, although again in this case the slope is slightly higher at the highest-resistance values.

In the case of the thinnest sample (340 Å) the amplitude of the periodic resistance oscillations was so small that the long-term stability of temperature was insufficient to allow complete families of curves as shown in Fig. 11. In this case it was found expedient to slowly traverse the resistance transition, plotting resistance versus temperature, and alternately switch the magnetic field from 0 to a value corresponding to $\phi_0/2$ (giving the greatest depression of T_c for the $n=0$ state). The result of this procedure is given in Fig. 14 and shows that over a sizable portion of the resistance transition the effect of the magnetic field is to shift the curve to lower temperature by a certain amount, which is reasonably independent of the value of resistance chosen.

Measurements were made on a 2900-Å indium film. Resistance versus magnetic field plots for a series of temperatures is shown in Fig. 15. The

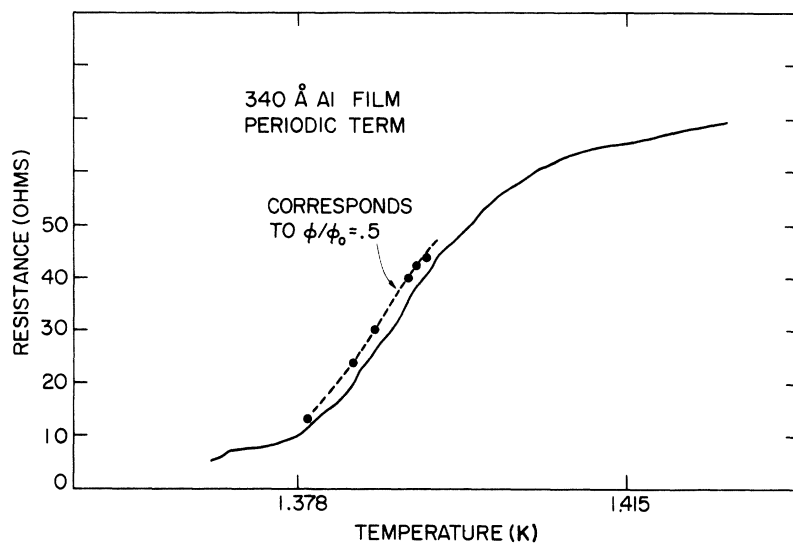


FIG. 14. Resistance versus temperature for $H=0$ and $H=\phi_0/2\pi R^2$ for a 340-Å aluminum film.

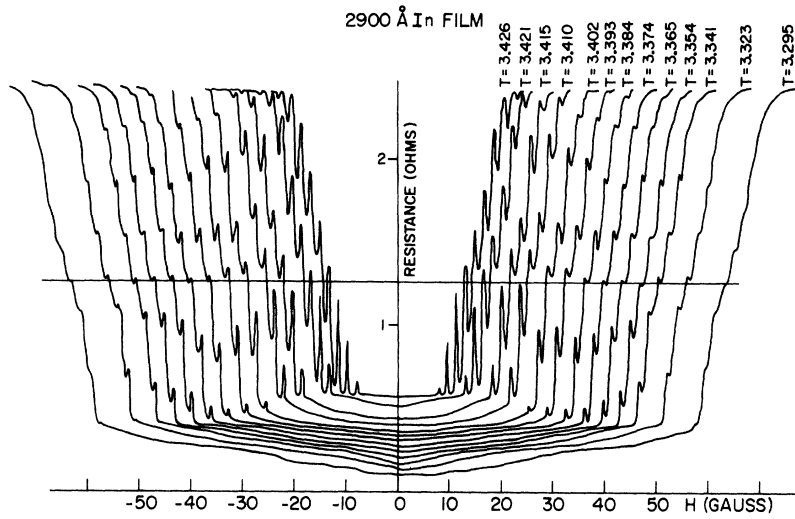


FIG. 15. Resistance versus magnetic field for a series of temperatures for a 2900-Å indium film. The horizontal line is for $R_N/2$.

line equal to $R_N/2$, one-half the normal resistance, is shown as the horizontal line. Using this resistance to define the phase boundary, values of H and T at maxima of T_c on the boundary were found. A plot of T_c versus H^2 is shown in Fig. 16 and is again a straight line. Figure 17 shows the displacement to lower temperature of the resistance transition for an applied field equivalent to $\phi_0/2$. Again we see that there is a unique value of the depression of T_c over most of the transition.

The aluminum films ranging in thickness from 2500 to 340 Å all gave qualitative agreement with the theory. The depression of T_c in the $n=0$ state and in the background curve was found in each case to be proportional to H^2 . The indium film also gave this result. Thus the qualitative agreement with Eq. (4) was excellent for all samples.

To make a quantitative comparison of theory and experiment we have calculated the penetration depth of the film at $T=0$, $\lambda_p(0)$, from the values of $\Delta T_c/H^2$ derived from plots of the background term and/or the periodic term such as given in Figs. 7-10, or

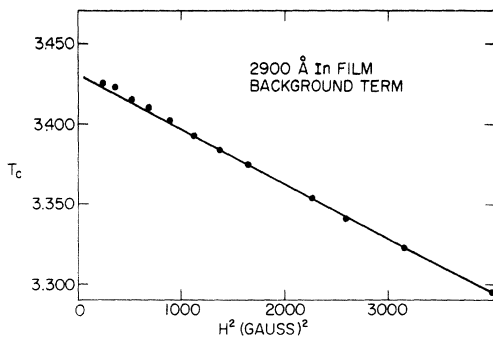


FIG. 16. $(T_c)_{\max}$ versus H^2 , 2900-Å indium film with phase boundary assumed to be at $R_N/2$.

16 and Figs. 12-14, 17. The value of the thickness used was that obtained from an interferometric measurement; the value of R used was that calculated from the periodicity of the ΔT_c with field, assuming the flux to be quantized in units of $hc/2e$. The value of $H_{cB}'(0)$ used was corrected from the bulk critical field, as explained in the theoretical summary, to take account of the increased transition temperature (and the corresponding increased binding energy of the superconducting pairs) in the film.

Table II gives a summary of the data from the various films and the values of the penetration depth calculated from the data according to theory. From the most recent and complete measurements, values of the penetration depth could be calculated from

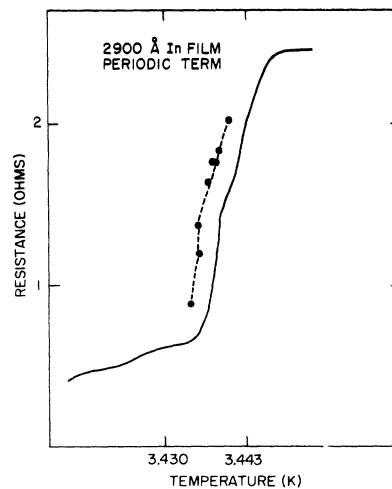


FIG. 17. Resistance versus temperature for $H=0$ and $H=\phi_0/2\pi R^2$ (dashed line) for 2900-Å indium film.

TABLE II. Summary of experimental results.

$d(\text{\AA})$	$T_c(K)$	$\Delta H(\text{Oe})$	$R(\mu)$	$H_{cB}^*(0)$	$\alpha_p = (-\Delta T_c/H^2)_p$	$\alpha_B = (-\Delta T_c/H^2)_B$	$\lambda_e(0)\text{\AA}$
Aluminum							
(a)							
340	1.394	2.44	1.64	124	8.0×10^{-4}	9.25×10^{-8}	{1950(P) 2170(B)}
370	1.374	1.17	2.38	122	2.53×10^{-3}	1.88×10^{-7}	{1600(P) 1670(B) 1570(H_c)}
1030	1.253	2.07	1.78	109	4.02×10^{-3}	3.58×10^{-6}	{1020(P) 1140(B)}
2500	1.219	3.38	1.40	104	2.51×10^{-3}	2.40×10^{-5}	{1050(P) 1110(B)}
(b)							
395	1.19	6.91	0.97	103	5.75×10^{-4}		1510(P)
495	1.22	3.33	1.41	105	{ 1.70×10^{-3} 1.54×10^{-3} }		{1270(P) 1340(P)}
620	1.269	3.53	1.37	111	1.85×10^{-3}		{1270(H_c) 1140(P)}
770	1.30	13.5	0.70	114	{ 5.7×10^{-4} 6.6×10^{-4} }		{1040(P) 960(P) 1010(H_c)}
1400	1.27	1.30	2.25	111	8.0×10^{-3}		910(P)
Indium							
2900	3.44	1.76	1.93	285	4.08×10^{-3}	3.25×10^{-5}	{695(P) 675(B)}

both the periodic term [designated (P)] and the background term [designated (B)]. These recent measurements include those for aluminum [in part (a)] in Table II and the one for indium. In addition are listed older measurements made on aluminum from which only the value of the periodic term could be used for calculating $\lambda_p(0)$. The reason for this was that in the early measurements the extreme care necessary in aligning the sample to obtain accurate values of the background curve was not ap-

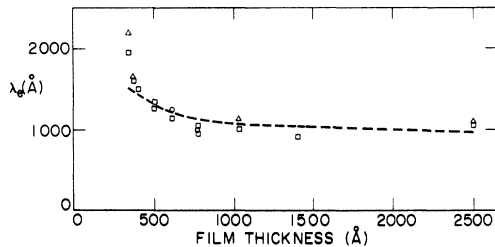


FIG. 18. Empirical penetration depth at $T=0$, $\lambda_p(0)$, for the aluminum films listed in Table II plotted as a function of their thickness. The values of $\lambda_p(0)$ were determined from the quadratic coefficient of the background term (triangle with dot), of the periodic term (square with dot), and from critical-field measurements at low temperature (circle with dot). The dashed curve is an attempt to fit the data with $\lambda_p(0) = \lambda_L(0)(\xi_0/\xi)^{1/2}$, where $1/\xi = 1/\xi_0 + 1/d + 1/l_0$ with $\xi_0 = 1.6 \times 10^{-4}$ cm, $l_0 = 1.0 \times 10^{-5}$ cm, and $\lambda_L(0) = 200$ Å.

preciated. In some cases the measured critical field at temperatures down to 0.87 K was also used to calculate $\lambda_e(0)$ [designated (H_c) in the table] from Eqs. (20) and (21).

The value of the radius R used in Table II was always calculated from the magnetic field period ΔH assuming the validity of the flux quantization relation $(\Delta H)\pi R^2 = \phi_0 = 2.068 \times 10^{-7}$ G cm². Although there is other evidence that this relation is exact, the diameter of one of the larger fibers was measured as accurately as possible in the optical microscope as an approximate check: Measured diameter of fiber + Al film equals 4.55 ± 0.1 μ ; Al film thickness is 0.143 ± 0.002 μ ; diameter of mid-point of film is 4.4 ± 0.1 μ ; diameter from flux quantization measurement is 4.49 ± 0.05 μ . The

TABLE III. Comparison of measured and theoretical values of α_p/α_B .

$d(\text{\AA})$	$R(\mu)$	α_p/α_B	$3R^2/d^2$	$(\alpha_p/\alpha_B)/(3R^2/d^2)$
Aluminum				
340	1.64	8.7×10^3	7.0×10^3	1.24
370	2.38	1.35×10^4	1.24×10^4	1.09
1030	1.78	1.12×10^3	0.90×10^3	1.25
2500	1.40	1.05×10^2	0.94×10^2	1.12
Indium				
2900	1.76	1.26×10^2	1.33×10^2	0.95

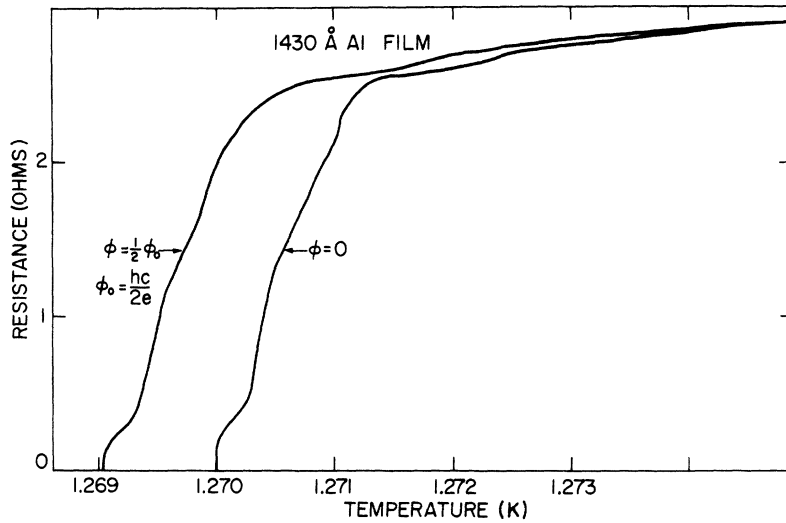


FIG. 19. Resistance versus temperature for a 1400-Å aluminum film for $H=0$ and $H=\phi_0/2\pi R^2$ show the constant depression of T_c , which was typical for the thicker films at all values of the resistance.

result verifies the flux quantization relation to an accuracy of about 3%.

Figure 18 shows the values of $\lambda_e(0)$ as determined experimentally as a function of the film thickness d . The values of $\lambda_e(0)$ obtained from the periodic term (square with dot), the background term (triangle with dot), and from the critical magnetic field at low temperature (open circle) are in reasonable agreement. In fact Fig. 18 implies that, for our evaporation procedure, $\lambda_e(0)$ approximates a single-valued function which monotonically increases as d decreases. The dashed curve is an attempt to fit the data with a function of the form

$$\lambda_e(0) = \lambda_L(0) (\xi/\xi_0)^{1/2},$$

where $1/\xi = 1/\xi_0 + 1/d + 1/l_b$. Here $\lambda_L(0)$ is assumed to be a constant independent of the thickness d and l_b is the bulk mean free path at 4.2 K. The dashed

curve is drawn for $\xi_0 = 1.6 \times 10^{-4}$ cm, $l_b = 1.0 \times 10^{-5}$ cm, and $\lambda_L(0) = 200$ Å. With this value of $\lambda_L(0)$, which is somewhat larger than the BCS theoretical value of 157 Å, the curve roughly represents the data except at the smallest values of thickness, where no values of the two parameters could make the data fit this functional form. For the thickest film (2500 Å) the mean value of $\lambda_e(0)$ was 1080 Å. This value agrees, within the probable error, with measurement of Groff and Parks⁷ for aluminum films (also 2500 Å thick), where the mean value of $\lambda_e(0)$ was 1107 Å.

Table III summarizes the comparison between the ratio of the measured quadratic coefficients α_p/α_B and the theoretical equivalent $3R^2/d^2$ given by Tinkham [Eq. (9)]. For aluminum films the results are in rather good agreement with theory, although the measured values are perhaps significantly higher than the theoretical ones. For the one indium sam-

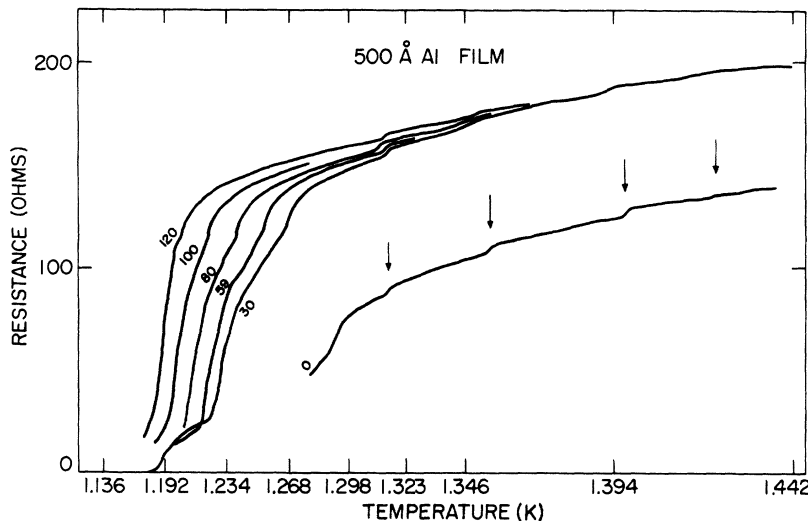


FIG. 20. Resistance versus temperature for various value of magnetic field. The numbers are mA in the solenoid and 120 corresponds to $\phi_0/2$. The $H=0$ curve has been displaced downward to show the step structure observed with this sample. Notice the temperature of the steps does not change with H .

ple the agreement between the measurements and theory is within the expected accuracy.

B. Additional Investigations

1. Form of Resistive Transition

To determine the transition temperature of the samples, the resistance was measured with a dc microvoltmeter using a measuring current of about $1 \mu\text{A}$. The procedure was to pump on the liquid-helium bath at a steady rate so that the temperature was gradually reduced through the temperature range of the superconducting transition. The resistance was plotted on an x - y recorder as a function of the vapor pressure of the liquid helium surrounding the sample. The electrical signal proportional to the vapor pressure was provided by a Baratron pressure gauge. The temperature was also measured with a resistance thermometer. After the sample became superconducting the temperature was gradually raised through the transition using a heater in the bottom of the Dewar to eliminate the effects of possible thermal nonequilibrium, because in the temperature region used the liquid helium was superfluid, and such irreversible effects were too small to be detected with reasonably slow temperature sweeps.

Figure 19 shows a typical measured transition for a fairly thick (1400 \AA) aluminum film. For this figure the pressure scale has been converted to a temperature scale. As was invariably found with aluminum films, the transition started as a gradual decrease in resistance at temperatures well above T_c for bulk aluminum (1.175 K). This effect was most pronounced in the films less than 500 \AA thick and in this case the depression in resistance would sometimes be noticeable at 4.2 K . After this gradual decrease in resistance the film resistance would fall suddenly to zero over a small range of temperature. For the sample of Fig. 19 this sudden drop in resistance took place in a temperature interval of about 1.3 mdeg . Sharp transitions of this sort were usually found in the thicker samples. In $500\text{-}\text{\AA}$ -thick samples the width of this part of the transition was usually of the order of 10 mdeg . It is to be noted that there is structure on the curve in addition to the expected smooth decrease of the resistance. When examined with sufficient temperature resolution, *all* samples showed such structure. Perhaps these irregularities are to be attributed to inhomogeneities in the samples near their ends where the aluminum film makes contact with the silver paint, although this is not certain.

For this particular film the application of a small magnetic field corresponding to $\phi_0/2$, that is, one-half of a flux quantum, simply displaces the curve to a lower temperature. This is typical for the thicker films. For the thinner films the resistance

transitions usually became steeper as the magnetic field was applied. This behavior is shown in Fig. 20 for a $500\text{-}\text{\AA}$ -thick film. The numbers on the curves refer to current through the solenoid producing the magnetic field; the field corresponding to $\phi_0/2$ is labeled 120. The curves were made by both raising and lowering the temperature so their shape could not be attributed to heating effects. This increase in the steepness of the resistance transition with field contrasts with that obtained in early experiments by Little and Parks,² in which the slope of the resistance transition decreased with increasing magnetic field. The probable explanation is that Little and Parks evaporated their films onto organic fibers whereas we used quartz fibers, the difference of the substrate being of greatest importance for the thinnest films.

Figure 20 also has a peculiar steplike structure as a function of temperature. This was reproducible in this particular sample but not found in others, although one or two steps were often observed. The explanation of this structure is unknown, but it should be noted that its position in temperature is independent of field. This is pertinent for the discussion below.

2. Search for Higher-Order Correlations

An essential idea of the BCS¹³ theory of superconductivity is that there are long-range correlations between pairs of electrons. The experimental result that flux is quantized in units of $hc/2e$ is very direct evidence of the correctness of this view be-

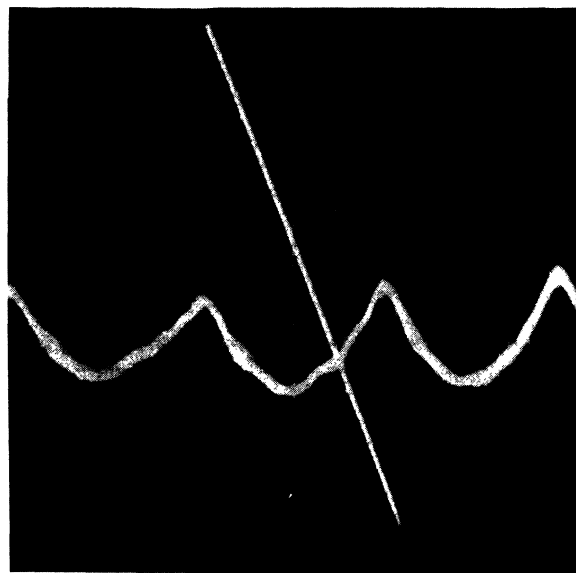


FIG. 21. Oscilloscope trace from Meyers and Little (Ref. 6) showing possible effect of higher-order correlations.

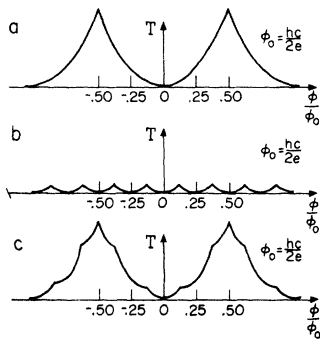


FIG. 22. Diagram showing conjectured T_c versus H for (a) pair correlations, (b) octet correlations, (c) pair correlations with an admixture of octet correlations.

cause of the factor 2 in the denominator, a fact that was pointed out by Onsager.²⁴ In the theory it is assumed that possible long-range correlations between more than two electrons, that is higher-order correlations, can be neglected. However, there is no theoretical evidence for or against the possibility that the untruncated Hamiltonian of a real superconductor might contain terms leading to higher-order correlations as well as pairs. Yang²⁵ has shown that if such higher-order correlations exist, they would be between even numbers of electrons and that flux quantization would take place with the flux quantum $= hc/Ne$, where N is the even number of correlated electrons in the basic unit. An interesting analogy suggested by Schrieffer²⁶ is the α -particle correlations in light nuclei.

In an early flux quantization experiment on small hollow cylinders of indium, Little and Parks observed the expected $hc/2e$ periodicity in the flux and in addition observed a weak $hc/8e$ periodicity superimposed on the basic curve. Figure 21 shows

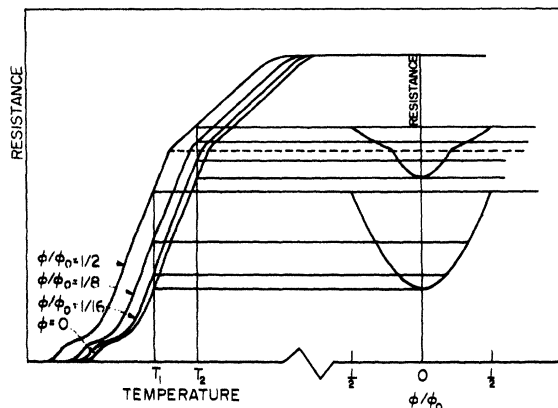


FIG. 23. Diagram showing how structure on a resistance versus temperature curve is transformed onto a resistance versus magnetic field curve.

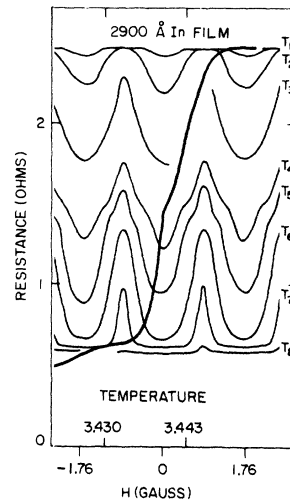


FIG. 24. Measured resistance versus H curve for 2900-Å indium film with superimposed resistance versus T at $H=0$ to show how the transformed structure is at the same resistance value in each case.

a photograph of their original oscilloscope trace. Figure 22 shows a schematic view of how an admixture of octet periodicity to the basic pair periodicity might have led to the experimental result.

In experiments with indium fibers we have observed effects that are very similar to those reported by Little and Parks. However, it appears that our results can be adequately explained by structure in the resistance transition and are not basically connected with the applied magnetic field. The way in which this happens in our experiments can be understood by referring to Fig. 23. On the left-hand side is an idealized plot (but not unlike those of real samples) of resistance versus temperature with magnetic flux as a parameter. If the temperature is held fixed at a value T_1 and the flux ϕ through the sample is varied from zero to $0.5\phi_0$, then the intersection of the vertical line T_1 with the transition curves gives the value of resistance for the corresponding values of flux. A plot of resistance versus flux, for fixed temperature T_1 , can be obtained and is shown as the expected parabolic plot in the (lower) right of the figure. However, if in the resistive transition there is a change of slope, as is often the case, the points of intersection corresponding to a temperature T_c lead to a resistance versus flux curve which is made up of two different parabolas. The net result is that as the magnetic field is swept, the structure of the resistance transition is reflected in the form of the resistance versus magnetic field curves.

In Fig. 24 is shown the superposition of the measured resistance transition in zero field and the resistance versus flux at constant temperature for the 2900-Å-thick indium sample which was analyzed in the previous section. The break in the R vs H curves takes place at about the same value of R as the break in the R vs T curves. In this case it is clear that the explanation of the structure in the R

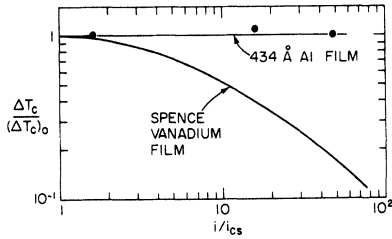


FIG. 25. Effect of measuring current i on the amplitude of the ($n=0$) periodic term for a 434-Å aluminum film compared to measurements on vanadium by Spence (Ref. 9). i_{cs} is the "critical" current suggested by Spence.

vs H curves has to do with the form of the resistive transition and cannot be interpreted as an effect of higher-order correlations.

This same sort of effect was always observed to some degree with aluminum films. An extreme example of such structure on the zero-field resistive transition is shown in Fig. 20. With this unusual sample we observed definite and reproducible steps in resistance superimposed on the resistive transition. Not surprisingly, plots of R vs H for this sample were correspondingly complicated. In all samples in which the structure of the R vs H curves was investigated, this structure could, in each case, be attributed to the structure on the R vs T curves. The exact cause of this structure remains obscure, but our conclusion is that R vs H structure observed in our experiments contains no evidence of higher-order correlations.

3. Effect of Transport Current

In discussing the theory no mention was made of

the transport current (parallel to the axis of the cylinder) which is used to measure the resistance changes caused by variations in magnetic field and temperature. Empirically, this is justified by the observation that, for the small measuring currents usually used, the resistance is not a function of the measuring current. On the other hand, with a large transport current we expect T_c and the resistance to depend on the current. In fact Spence⁹ observed a "critical" transport current i_{cs} in flux quantization experiments on vanadium cylinders. For currents above a critical value, the depression of T_c due to H approached zero rapidly (see Fig. 25). This fact seems to explain the curious absence of flux quantization oscillations in vanadium cylinders reported by Meyers and Little,⁶ since measuring current in these earlier experiments was well above the critical value.

It was conjectured by Spence that this critical transport current corresponded to the situation where the de Broglie wavelength of the carriers of the transport current was comparable to the circumference of the cylinder; that is, $\lambda_D = h/mV_d \approx 2\pi R$, where R is the cylinder radius and V_d is the drift velocity of the carriers of the transport current.

The critical current i_c for the destruction of superconductivity corresponds to the de Broglie wavelength approximately equaling the temperature-dependent coherence distance, that is, $\lambda_D = \xi(T)$. As both i_{cs} and i_c are inversely proportional to their respective λ 's, we have $i_{cs}/i_c = \xi(T)/2\pi R$. Using the Bardeen expression for the critical current density j_c and taking $i_{cs} = 2\pi R d j_c$, where d is the film thickness, one obtains $i_c = 20 H_{cB}^2(T) \xi(T) d / 3 \sqrt{3} \phi_0$. Using the empirical temperature dependence for

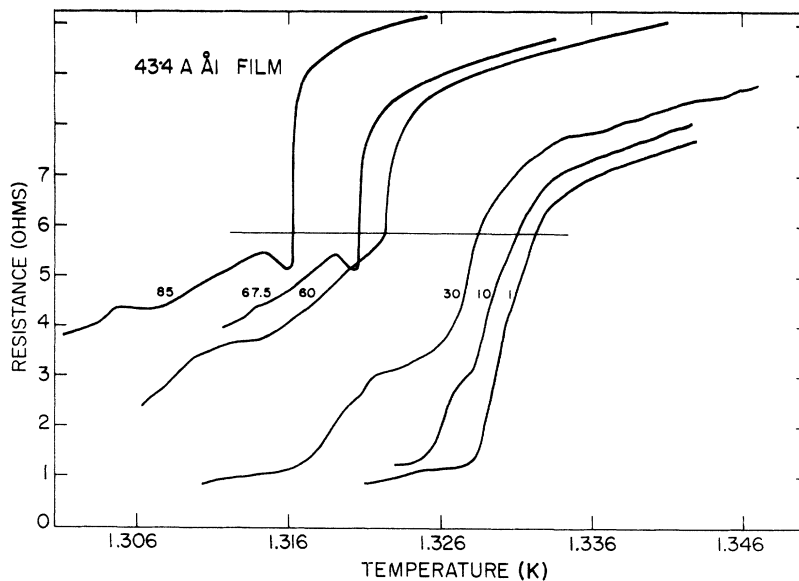


FIG. 26. Resistance of 435-Å aluminum film versus T for measuring currents (μA). For high measuring currents the steep part of the resistance transition shifts to lower temperatures, becomes much steeper, and finally develops a resistance minimum.

$H_{cB}(T)$, and $\xi_0/(1 - T/T_c)^{1/2}$ for $T_c - T \ll T_c$, and the mean free path $l \approx d$, one obtains

$$i_c = \frac{80H_{cB}^2(0)\xi_0 d^2 \Delta T}{3\sqrt{3}T_c\phi_0}.$$

According to Little and Spence, ΔT should be taken approximately equal to $(\Delta T_c)_0$, maximum depression of ΔT_c for very small transport current i , as determined in the experiment.

We tried to observe this effect in an aluminum cylinder of radius $R = 3.20 \mu$ and film thickness $d = 434 \text{ \AA}$ whose calculated critical current i_{c3} was $0.6 \times 10^{-6} \text{ A}$. Figure 25 shows a measurement of $(\Delta T_c)_{\text{max}}$ as a function of the measuring current using a constant resistance equal to one-half of the normal resistance. Apparently the effect observed for vanadium cylinders was not present in the aluminum cylinders at this current density. The measured value of $(\Delta T)_{\text{max}}$ up to about $50 \mu\text{A}$ did not significantly change, even though the calculated critical transport current i_{c3} was $0.6 \mu\text{A}$.

Although we did not observe the expected "critical current" we did observe an unusual effect with this film. Figure 26 shows the resistance plotted as a function of temperature for different values of transport current (the numbers on the curves correspond to the current in μA). The form of the resistance transition is strikingly altered by the current. The steep drop in resistance is displaced to lower temperatures by higher currents as would be expected. In addition to this temperature displacement, the width of the rapid drop in resistance decreased drastically from a width of $5 \times 10^{-3} \text{ K}$ to about 10^{-4} K , a factor of 50 times. In addition, there developed a minimum on the resistance vs temperature curve. It should be mentioned that all of these curves were stable and reversible at all temperatures and currents, and thus not to be explained by irreversible heating effects which are often seen in critical current measurements. The extreme sharpness of the transition at high currents is perhaps to be explained by a reversible heating effect. However, it is not easy to see how such an effect would lead to the minimum in the resistance curve.

If we arbitrarily take the resistance level shown by the horizontal line in Fig. 26 to define the transition temperature, we can compare the measured critical current as a function of temperature with the Ginzburg-Landau theory which predicts $I_c^{2/3}(T) \sim T_c(0) - T_c(I)$. This function is shown by the dashed line in Fig. 27 and fits the values of I_c well below $T_c(0)$. However, near $T_c(0)$ the measured critical current drops below the theoretical curve. Such behavior of the critical current has been observed in aluminum thin-film bridges and a depression of the transition temperature of

about what was found here has been attributed to fluctuations near T_c .²⁷ Although the result is suggestive of fluctuation effects, no definite conclusions can be made without further measurements.

4. Effect of Fluctuations

If fluctuations are present at T_c it seems reasonable that the effective shape of the phase boundary might be noticeably affected. Presumably any such effect would be expected to show up most at high-resistance levels and for a low measuring current. For most of the samples the theoretical prediction of intersecting parabolas [Eq. (4)] was found to hold within the limit of error over a fairly wide range of resistance. However, for one sample ($d = 620 \text{ \AA}$, $R = 0.97 \mu$), the depression of T_c (for $n = 0$) was not proportional to H^2 for resistances above half of the normal resistance. The measured depression of T_c is shown in Fig. 28. The depression at higher fields is much less than we expect from the parabolic law. Since there is strong evidence that fluctuation effects are present in the transitions of thin aluminum films²⁷⁻²⁹ we present the following qualitative explanation for this result.

The theory summarized in Sec. I neglects fluctuation effects and derives a simple parabolic curve of the lowering of T_c with H . Inclusion of fluctuation effects would give the phase transition a finite width. In addition we would expect a rounding of the intersection of the parabolas from neighboring angular momentum states for the following reason. Consider a region in the normal state, but close to the phase boundary, say, near the region where $\phi/\phi_0 = 0$. There will be a certain probability for a given volume fluctuating into the superconducting state, which will lead to a lowering of the resistance and, if we chose to interpret it

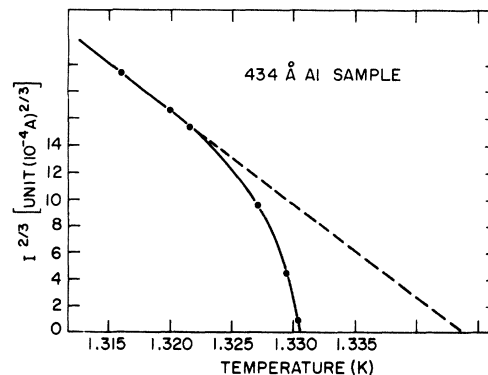


FIG. 27. $(\text{Critical current})^{2/3}$ versus temperature for 434- \AA aluminum film. Dashed line shows the fit to the Ginzburg-Landau theory at low temperatures. Measured deviation may be the result of fluctuations.

so, a raising of the effective T_c . Now consider a point near the phase boundary close to the intersection of two angular momentum states $\phi/\phi_0 \approx 0.5$. Since two superconducting states are equally close and presumably each has the same probability, the chance of fluctuating into the superconducting state should be doubled. This would lead to a greater decrease in resistance in this area than expected and thus a smaller decrease in T_c than parts of the phase boundary where only one state is available. The expected rounding of the transition is suggested by the dashed line (Fig. 29).

Qualitatively this explanation is consistent with the measurements of Fig. 28. The question remains as to why the effect was seen only in this particular film. Of the films in which T_c was carefully measured as a function of H for $n=0$, this film was one of the thinnest and was the one with the smallest radius. This latter fact was perhaps important because the amplitude of the voltage oscillations with H increases rapidly as R decreases. This meant that the measuring current required could be made small and the detection of flux quantization effects could be measured higher on the transition curve where the slope was much less and where fluctuations should be significant. On most samples it was necessary to stay on the steep part of the transition curve to obtain the required sensitivity and in this region the mean-field approximation to fluctuation theory is no longer valid and so comparison with theory is not possible.

V. DISCUSSION

The experimental results summarized in Table II show basic agreement with theory for very thin

films as well as thick films. The penetration depth at $T=0$ as calculated from both the periodic term and the background term is nearly a monotonic function of film thickness, increasing rapidly in the thinnest films. This is the general behavior we expect when mean free path and film thickness effects are taken into account as is shown by the dashed line in Fig. 18 if we assume $\lambda_L(0)=200$. This value for $\lambda_L(0)$ is, of course, considerably larger than the theoretical value of 157 \AA predicted by the BCS theory. On the other hand the values of $\lambda_g(0)$ obtained by the measurements are close to those obtained from other measurements of $\lambda_g(0)$ including the present measurements of critical field at low temperatures. The thinner films also agree with separate measurements on plane thin films of aluminum by Tedrow and Meservey.³⁰

The comparison in Table III between α_p/α_B and $3R^2/d^2$ shows that when the material parameters are eliminated these measured ratios are equal, as predicted by theory, within about 15%. This error is probably accounted for by errors in the values of α_p and d^2 , although it is possible that the consistently larger ratio of α_p/α_B is significant for aluminum. The ratio for indium is within the expected error for this measurement.

A minor discrepancy between measurements and theory is the amplitude of the variations in T_c for higher quantum numbers. The measured amplitude is less than the predicted. It is at least partly because of this effect that the local maxima in T_c disappear in the experimental curves much before it is predicted. For instance, in Fig. 6 the maxima have disappeared by $n=70$ whereas from Eq. (12) and Table III we expect

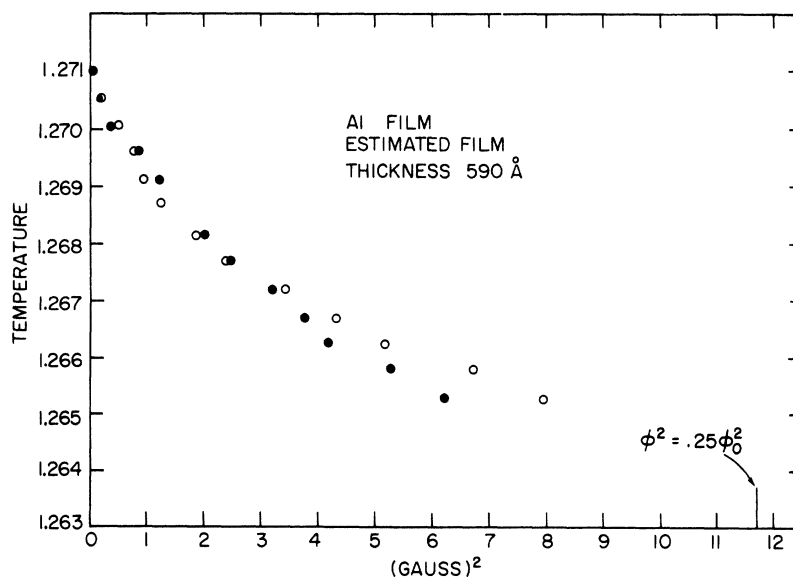


FIG. 28. T_c versus H^2 for 620-Å aluminum film for high value of resistance ($R=0.8R_N$). Measurements for positive and negative H are shown by open and solid points. Deviation from a straight line is perhaps caused by fluctuations.

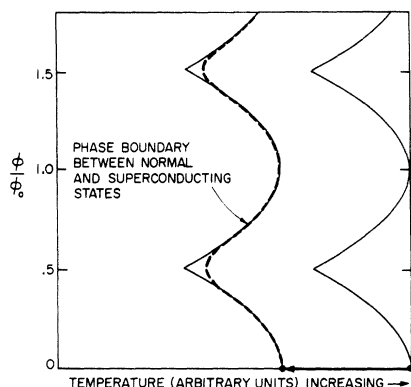


FIG. 29. Diagram showing the theoretical phase boundary without fluctuations (solid) and conjectured boundary with fluctuations (dashed).

this not to happen until $n = 450$. This effect was not caused by inaccurate alignment of the sample holder with the field. However, it is possible that the sample itself may be very slightly bowed or tapered, although there was no other evidence to support either of these two possibilities. A more fundamental possibility is that the transition between angular momentum states of high quantum number is not entirely sharp.

Apart from these rather minor discrepancies, the agreement with theory can be considered excellent for all the films. For the thickest film (2500 Å) the results agree with those of Groff and Parks⁷ on 2500-Å aluminum films. For the thin films the agreement with theory is still very good, even when the width of the resistive transition is very much greater than the change in T_c caused by a magnetic field corresponding to one-half flux quantum. This is particularly striking for the 370-Å film which had the comparatively large ra-

dius of 2.38μ . Here the depression of T_c at $\phi = \phi_0/2$ was only 0.9×10^{-3} K whereas the transition width was about 10 times this value. Thus in both limits of $(\Delta T_c)_p$, large and small compared with the width of the resistive transition, the measurements agree well with theory.

No evidence was found for the existence of higher-order correlation effects. Although structure was invariably seen on the T_c vs H curves in addition to the parabolic curves, this structure was, in all cases investigated, traceable to structure on the R vs T curves for $H = 0$ and could therefore have no bearing on the question of higher-order correlations.

Evidence of the effect of fluctuations was observed both in the deviation of the critical current from the Ginzburg-Landau mean-field theory and from the rounding of the minima of the T_c vs H curve in at least one sample. Since it now seems to be established that fluctuation effects do exist in thin aluminum films it should be possible to use the theoretical value of the resistance $R = R(H, T - T_c)$ from fluctuation theory to calculate the value of R as a function of H and T . This would eliminate the somewhat unsatisfactory comparison of theoretical variations of T_c with the experimentally determined T_c defined by some arbitrary fraction of the normal resistance. Actually, however, the present investigation shows that unless we select some extreme case in which the fluctuations are maximized, the simple theory is very satisfactory. Also it must be appreciated that introduction of fluctuations will complicate the theory considerably. Since the fluctuations sample states away from T_c , where the supercarrier concentration is not zero, the assumptions of zero carrier concentration everywhere in the cylinder and no variation of the magnetic field are no longer valid.

*Research supported by the NASA Electronics Research Center.

†Present address: San Francisco State College, San Francisco, Calif.

‡Supported by the U. S. Air Force Office of Scientific Research.

¹W. A. Little and R. D. Parks, Phys. Rev. Letters **9**, 9 (1962).

²R. D. Parks and W. A. Little, Phys. Rev. **133**, A97 (1964).

³R. Doll and M. Näbauer, Phys. Rev. Letters **7**, 51 (1961).

⁴B. S. Deaver, Jr. and W. M. Fairbank, Phys. Rev. Letters **7**, 43 (1961).

⁵W. Little, Rev. Mod. Phys. **36**, 264 (1964).

⁶L. Meyers and W. A. Little, Phys. Rev. Letters **11**, 156 (1963); **13A**, 325 (1964).

⁷R. P. Groff and R. D. Parks, Phys. Rev. **176**, 567 (1968).

⁸R. Meservey and L. Meyers, Phys. Letters **26A**, 367 (1968).

⁹S. T. Spence, Ph.D. thesis (Stanford University, 1967) (unpublished).

¹⁰M. Tinkham, Phys. Rev. **129**, 2413 (1963).

¹¹D. H. Douglass, Jr., Phys. Rev. **132**, 513 (1963).

¹²C. Delmasso and E. Pagiola, Nuovo Cimento **35**, 311 (1965).

¹³J. Bardeen, L. N. Cooper, and J. R. Schrieffer, Phys. Rev. **108**, 1175 (1957).

¹⁴P. B. Miller, Phys. Rev. **113**, 1209 (1959).

¹⁵P. G. de Gennes and M. Tinkham, Physics **1**, 107 (1964).

¹⁶J. Strong, *Procedures in Experimental Physics* (Prentice-Hall, Englewood Cliffs, N.J., 1938).

¹⁷E. I. duPont de Nemours and Co., Wilmington, Del.

¹⁸Alpha Metals, Inc., 56 Water Street, Jersey City, N.J.

¹⁹Allegheny Ludlum Steel, Breckenridge, Pa.

²⁰C. Blake, C. E. Chase, and E. Maxwell, *Rev. Sci. Instr.* **29**, 715 (1958); C. Blake and C. E. Chase, *ibid.* **34**, 984 (1963).

²¹Wallace and Tiernan, Belleville, N.J.

²²MKS Instruments, Inc., Burlington, Mass.

²³Keithley Instruments, Cleveland, Ohio.

²⁴L. Onsager, *Phys. Rev. Letters* **7**, 50 (1961).

²⁵C. N. Yang, *Rev. Mod. Phys.* **34**, 694 (1962).

²⁶J. R. Schrieffer, *Superconductivity* (Benjamin, New

York, 1964), p. 256.

²¹W. E. Masker, S. Macelja, and R. D. Parks, *Phys. Rev.* **188**, 745 (1969); W. E. Masker and R. D. Parks, *Phys. Rev. B* **1**, 2164 (1970).

²⁸P. M. Tedrow, R. Meservey, and B. B. Schwartz, *Phys. Rev. Letters* **24**, 1004 (1970).

²⁹J. E. Crow, R. S. Thompson, M. A. Klenin, and A. K. Bhatnagar, *Phys. Rev. Letters* **24**, 371 (1970).

³⁰P. M. Tedrow and R. Meservey (unpublished).

PHYSICAL REVIEW B

VOLUME 4, NUMBER 3

1 AUGUST 1971

Thermal Conductivity and Ultrasonic Attenuation in Clean Type-II Superconductors

A. Houghton*

Department of Physics, Brown University, Providence, Rhode Island 02912

and

K. Maki

Department of Physics, Tohoku University, Sendai, Japan

(Received 4 January 1971)

We calculate the thermal conductivity and low-frequency ultrasonic attenuation in clean type-II superconductors in the high-field region. Use is made of a Green's function due to Brandt, Pesch, and Tewordt which enables accurate calculation of the transport properties in the vicinity of the upper critical field. It is shown that in the low-temperature limit the transport coefficients are simple functions of a single parameter $\mu = 2\sqrt{\pi} (\Delta/k_c v_F)^2 k_c l$, where Δ^2 is the spatial average of the square of the order parameter, k_c is the reciprocal-lattice vector of the vortex lattice, v_F is the Fermi velocity, and l is the electronic mean free path.

I. INTRODUCTION

It is now recognized that there is a remarkable difference between the dynamical properties of dirty ($l \ll \xi_0$, where $l = v_F \tau$ is the electronic mean free path and ξ_0 is the pure-superconductor coherence distance) type-II superconductors in high magnetic fields and those of clean ($l \gg \xi_0$) type-II superconductors in high magnetic fields. In the dirty case, it is found experimentally that the change in the transport coefficients (for example, the ultrasonic attenuation and thermal conductivity) near H_{c2} is proportional to $H_{c2} - B$. This behavior is readily understood in terms of gapless superconductivity.¹ On the other hand, in clean type-II superconductors the change appears² to scale as $(H_{c2} - B)^{1/2}$; further, even though $l \gg \xi_0$, the transport coefficients are strongly dependent on mean free path.

In this paper, we determine the transport coefficients of clean type-II superconductors near H_{c2} by a method which makes use of the single-particle propagator recently derived by Brandt *et al.*³ The method has so far only been used to determine high-frequency response functions; for example, the ultrasonic attenuation at high frequency has been

calculated by Cerdeira and Houghton,⁴ and the complex conductivity in the extreme anomalous limit was determined by Hibler and Cyrot.⁵ In both these cases, calculation is considerably simplified by noting that the energy integral over the product of Green's functions can be well approximated by essentially a product of the densities of initial and final states. However, as yet, there has been no experimental work under these conditions, and, therefore, no direct check on the validity of the calculations. In this paper, we show that it is possible to derive simple analytical expressions for the transport coefficients in the low-frequency limit. We calculate both the thermal conductivity and the ultrasonic attenuation and show that the predictions of the theory are consistent with the main features of the experimental results.

II. GENERAL FORMULATION

The response functions for clean type-II superconductors near H_{c2} can be expressed in terms of Brandt's Green's functions as

$$Q_{AB}(\omega_m) = T \sum_n \int \frac{d^3 p}{(2\pi)^3} A_{p, p+a} B_{p, p+a}$$

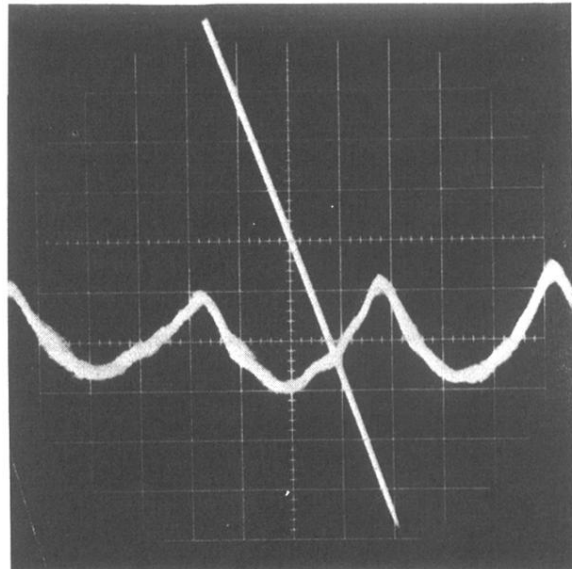


FIG. 21. Oscilloscope trace from Meyers and Little (Ref. 6) showing possible effect of higher-order correlations.